

The Effects of Graphene Oxide and Iron Oxide (II) Co-addition on Properties of a Polypropylene/high-density Polyethylene Blend

Daniel Felipe Pietezak^a, Teresa Tromm Steffen^a, Luis César Fontana^a ,
Carla Dalmolin^a , Daniela Becker^{a*} 

^aUniversidade do Estado de Santa Catarina, Centro de Ciências Tecnológicas, Joinville, SC, Brasil.

Received: December 14, 2023; Accepted: February 14, 2024

This study investigated the impact of adding graphene oxide (GO) and iron oxide (II) (Fe_3O_4) nanoparticles individually and in combination on the morphology, thermo-mechanical, and dielectric properties of a Polypropylene/High-Density Polyethylene (PP/HDPE) blend. By adding these nanoparticles separately or as a mixture, we can determine if both mechanisms have a synergistic effect and how they impact the dielectric constant values of their nanocomposites. The nanoparticle mixture was prepared in both an alkaline and a neutral medium. The mixture in the alkaline medium contained lower quantities of iron nanoparticles than in the neutral medium, and they were localized on the surface of GO. The nanocomposites showed significant differences in dynamic-mechanical and dielectric properties. The system with Fe_3O_4 exhibited a higher storage modulus, while the system with GO had a higher dielectric constant. However, no synergistic effect was observed in the nanoparticle mixtures.

Keywords: Dielectric properties, nanocomposites, graphene oxide, iron oxide (II).

1. Introduction

Dielectric materials are used in capacitor fillings and have the function of isolating the capacitor's electrodes. This separator element must meet specific properties such as flexibility, resistance to electrolyte corrosion, and dielectric properties such as high ionic and low electrical conductivity in a wide operating range (avoiding short-circuit problems), all with a small thickness¹. The separators in standard capacitor systems are, in general, made of a blend of polypropylene (PP) and polyethylene (PE) due to some characteristic aspects besides the insulating characteristic, such as easy processing and recyclability, mechanical, thermal, and chemical stability². Although such desired properties, other factors should be improved in the PP/HDPE system, such as a high dielectric capacity, high resistivity, and low dielectric loss³.

Both graphene oxide (GO) and iron oxide (II) (Fe_3O_4) have similar properties in terms of enhancing dielectric properties since the carbon nanoparticles tend to add interfacial polarization mechanisms⁴, and the Fe_3O_4 introduces dipoles in the original polymer matrices⁵. As an example of such behavior change, studies in high frequencies show that these mechanisms can be combined when both nanoparticles are mixed to obtain Fe_3O_4 /GO nanocomposites⁶. The literature has shown that adding 1% of that mixture into polymer blends of polyvinyl alcohol (PVA) and poly(3,4-ethylenedioxythiophene) can produce a nanocomposite with potential properties of electronic compounds and electromagnetic shielding^{7,8}. A similar property enhancement was verified in the epoxy polymer matrix⁹ and in polyvinylidene fluoride (PVDF)¹⁰, to which mechanical properties, thermal stability, and the

dielectric constant improvements were observed. To this end, the nanoparticles can seemingly act by introducing new mechanisms of interfacial and dipole polarizations (depending on time and temperature) into the immiscible polymer matrix and changing the initially isolated properties of the polymer chain into a semiconductor state⁶. As a result, these nanocomposites have a wide range of applications, such as high-frequency or embedded capacitors⁴, heat transfer improvement in nanofluids¹¹, and high absorption devices⁸. To our knowledge, the influence of the simultaneous addition of graphene oxide and iron oxide in the PP/HDPE blend, especially in the dielectric properties, has not yet been studied.

So, this work aims to evaluate the influence of adding individually and mixed graphene oxide and iron oxide in the morphological, thermal, mechanical, and, especially, dielectric properties of a high-density polyethylene/polypropylene polymer blend. In order to understand the effect of polarization and dipole mechanisms brought by graphene oxide or iron oxide on the PP/HDPE matrix, these nanoparticles were added separately or as a mixture into the polymer blend. The results are compared to evaluate whether there is a synergic effect between both mechanisms and how they affect the dielectric constant values of their nanocomposites.

2. Experimental Procedures

2.1. Materials

Two polymers were chosen for this work, the heterophase copolymer of ethylene-propylene (PP) as the continuous phase and high-density polyethylene (HDPE) as the dispersed

*e-mail: daniela.becker@udesc.br

phase, both purchased from Braskem, with grades CP 741 and HC7260LS-L, respectively. The graphene was purchased as a powder from Chengdu Organic Chemistry (China) with purity above 99% and thickness from 4 nm to 20 nm. The iron oxide (II) was acquired as a powder from Sigma Aldrich, with a purity of 97%, size between 50 nm and 100 nm, and spherical geometry, according to the datasheet from the manufacturer. All materials were used as received, apart from the graphene that underwent an oxidation process.

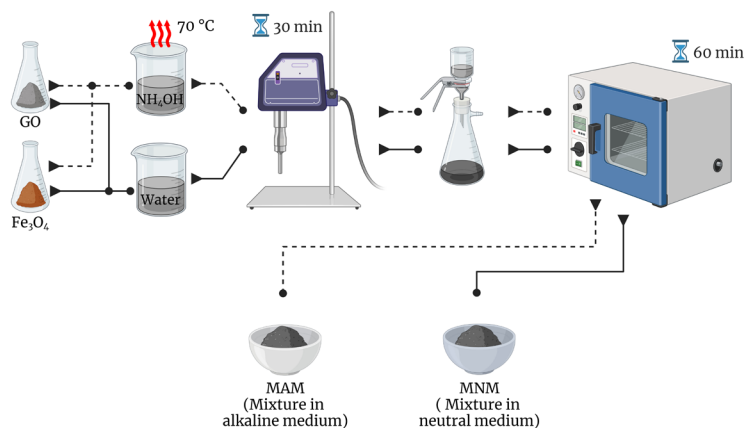
2.2. Preparation of nanoparticles

Graphene oxide was prepared from the graphene through the modified Hummers' Method¹². For this end, the graphene was initially put in a mixture of potassium permanganate, sulfuric acid, and phosphoric acid (6:9:1) and stirred for

12 h until the solution turned dark brown. After that, the resulting nanoparticle was filtered and dried at 60°C for 24 hours in an air circulation oven.

Two different methods were used to obtain the nanoparticle mixture between graphene oxide and iron oxide. The first method was based on another work¹¹ and called a mixture in alkaline medium (MAM): both nanoparticles, in the proportion of 1:1, were added in a recipient with ammonium hydroxide, heated at 70 °C for 30 min, sequentially, sonicated for another 30 min, and finally filtered. The second mixture method, namely mixture in neutral medium (MNM), was performed through simple water sonication for 30 min and subsequent filtration. Both mixtures were oven-dried for 1 hour at 60 °C. Figure 1a shows the procedure to obtain these mixtures.

a) Preparation of nanoparticles mixtures



b) Preparation of blends and nanocomposites

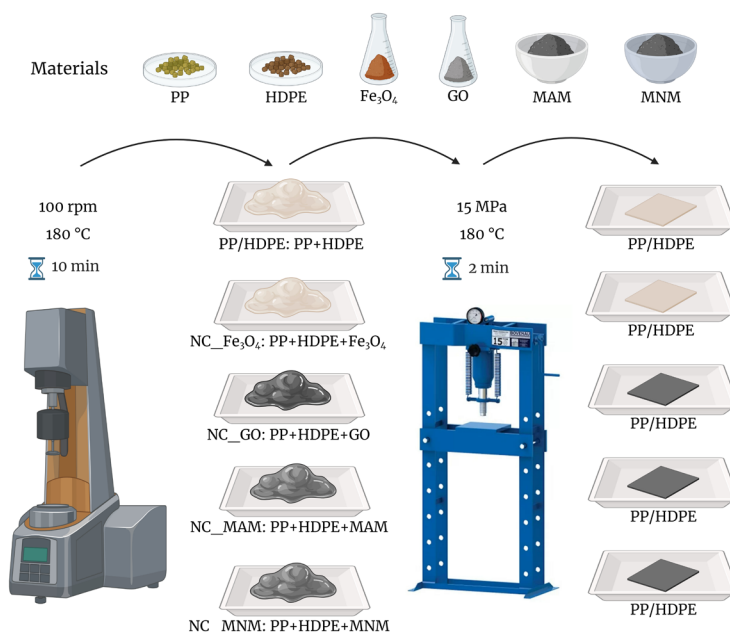


Figure 1. Schematic representation a) of the procedures conducted to obtain the mixtures between graphene oxide and iron oxide; and b) of the steps to obtain blend and nanocomposites samples. Created with BioRender.com

2.3. Processing of nanocomposites

The HDPE and the PP were previously dried at 100 °C in a circulating-air stove to eliminate all residual water before processing. The blend proportion was 90/10 (PP/HDPE), and a composition of 1% in mass of the nanoparticles, i.e., iron oxide (II), graphene oxide, bands (MAM) or mixture in neutral medium (MNM), was chosen to produce the nanocomposite samples. Both polymers were mixed using the torque rheometry technique (Thermo Scientific Haake Rheomix 600) at 180 °C, 100 rpm for 10 min, in which nanoparticles were added individually or as mixtures to the polymers. Films of the produced polymer nanocomposites were obtained through the hot-molding press (Bovenau P15 ST) at 180 °C and under 15 MPa for 2 min and cooled instantaneously to room temperature, which led to samples with an average thickness of 0.18 mm. That process is graphically represented in Figure 1b. Table 1 summarizes the sample names of each nanocomposite, having the PP/HDPE blend as a matrix.

2.4. Characterization

Graphene and Oxide graphene were characterized by Fourier Transform Infrared (FTIR), X-ray diffraction, and X-ray Photoelectron Spectroscopy (XPS). The nanoparticle mixtures were characterized by Transmission Electron Microscopy (TEM) and X-ray Photoelectron Spectroscopy (XPS). FTIR spectra were obtained with KBr using 12 scans in the range from 4000 cm⁻¹ to 550 cm⁻¹, with a resolution of 4 cm⁻¹, in a Spectrum One B Perkin-Elmer. The Shimadzu XRD 6000 equipment performed the x-ray diffraction test using monochromatic Cu radiation (0.154 nm). The measurements were performed from 5° to 70°, with a standard operating rate of 2°/min. XPS analyses were conducted in a Thermo Scientific XPS (Al-K α , $h\nu = 1486.6$ eV). Survey spectra were collected from -10 eV to 1350 eV after ten scans, with a pass energy of 200.000 eV, a step size of 1.000 eV, and a dwell time of 10.000 ms. The base pressure was set to 10⁻⁸ mbar, and the X-ray spot was 400 μ m in diameter. A charge compensation gun (flood gun) was utilized during the analysis. Data were collected from three different surface points in each sample. The chemical composition was obtained through the “speciation” function available on the Avantage® software from Thermo Scientific. For the transmission electronic microscopy analysis, the nanoparticles were dispersed in acetone, sonicated for 2 min, and then characterized in a JEM 2100 JEOL microscope.

The blend morphology was studied through electronic scanning microscopy with field emission (FEG-SEM) using a JSM 6701F-JEOL at 10 kV. The samples were submerged

Table 1. Sample's name an indication of dispersed phase of the nanocomposites with PP/HDPE as matrix.

Sample name	Dispersed phase
PP/HDPE	-
NC_Fe ₃ O ₄	Iron oxide II as purchased
NC_GO	Graphene oxide produced
NC_MAM	Mixture in alkaline medium
NC_MNM	Mixture in neutral medium

in N₂ for 5 minutes, and the cryo-fracture surfaces of the different samples were coated with a gold layer.

The dynamic-mechanical analysis (DMA) was carried out to observe how the nanoparticles affected the mechanical properties of the final nanocomposites through the analysis of the storage modulus (E') and the glass-transition temperature (T_g). The experiments were performed with a Netzsch DMA 242 E in the stress-strain mode under a nitrogen atmosphere, with a temperature range from -150 °C to 50 °C, considering a frequency of 1 Hz and a heating rate of 3 °C/min.

The effect of the samples' processing and composition on the crystallization temperature (T_c) and the crystallization degree (%) were analyzed using differential scanning calorimetry (DSC) on a Netzsch Maia-230. The samples were submitted to heating and cooling cycles under an N₂ atmosphere. Heating from 25 to 225 °C was applied at a 10°C min⁻¹ rate, keeping in isotherm for 2 min. Cooling was then carried out down to 25 °C at a 20 °C min⁻¹ rate, keeping in isotherm for 2 min, followed by a second heating of 10°C min⁻¹ up to 350 °C. The degree of crystallinity, X_c , was calculated from Equation 1, in which ΔH and $\phi \cdot \Delta H_0$ are, respectively, the enthalpy obtained through DSC and for the theoretical 100 % crystalline polymer, and ϕ indicates the fraction of each polymer in the blend. The values used for ΔH were 287 J/g for HDPE and 207 J/g for PP¹³.

$$X_c = \left[\frac{\Delta H}{\phi \cdot \Delta H_0} \right] \cdot 100 \quad (1)$$

The electrochemical impedance spectroscopy (EIS) analysis was carried out to see how the dielectric constant was affected by the nanomaterials due to new polarization mechanisms brought to the polymer matrix of the nanocomposites. This study used a potentiostat/galvanostat coupled to a frequency analyzer module (Gamry 1010e) with the blocking electrode method. Tests were carried out at open circuit potential and room temperature, in which a thin film of each sample was sandwiched between two stainless steel electrodes, applying an AC potential of 10 mV (rms) in the frequency range between 10 kHz and 1 Hz. Dielectric constant data were calculated from impedance parameters using Equation 2, in which ϵ' indicates the real part of the electrical permittivity, and ϵ'' are, respectively, the real and imaginary impedances achieved through the analysis, ω is the frequency, and A and d express the geometric characteristics of area and thickness of the polymer film.

$$\epsilon' = \frac{-Z'}{2\pi f \epsilon_0 Z^2 \frac{A}{d}} \quad (2)$$

3. Results and Discussion

3.1. Characterization of graphene and graphene oxide

Figure 2 presents FTIR spectra for graphene and graphene oxide. The graphene spectrum has three characteristic bands,

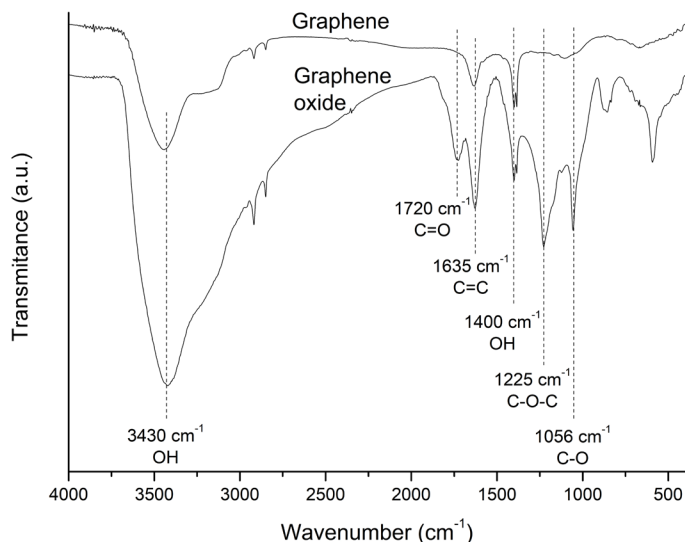


Figure 2. FTIR spectra for graphene and graphene oxide.

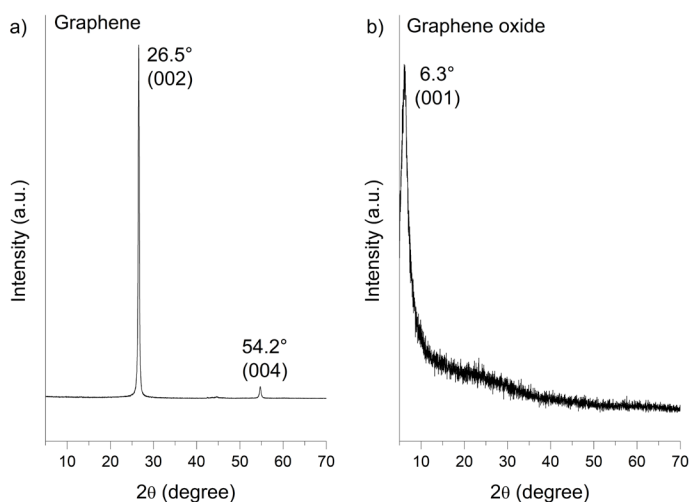


Figure 3. X-Ray diffraction spectra for a) graphene and b) graphene oxide samples.

at 3430 cm^{-1} , 1635 cm^{-1} , and 1400 cm^{-1} , assigned, respectively, to the stretching mode of O-H bonds, stretching vibrations of C=C, and deformation of hydroxyl groups¹². These same bands are present in the graphene oxide spectrum, and new ones that characterize this type of material appear as hydroxyl, carboxyl, and epoxide groups. At 1720 cm^{-1} , the peak is assigned to the stretching vibration of carbonyl groups (C=O); at 1225 cm^{-1} , it denotes C-O-C stretching, and the peak at 1056 cm^{-1} corresponds to the vibrational mode of the C-O group^{12,14,15}. All those bands' presence confirms Hummers' Method's efficacy in oxidizing the graphene.

Figure 3 shows the diffraction pattern for graphene (a) and graphene oxide (b) samples. The sharp peak at 26.5° (002) for the graphene sample indicates an interplanar distance of 3.4 \AA , obtained through Bragg's Law. Despite this length being in accordance with the one referred to in the literature for graphene, the peak at 26.5° is not typical for graphene sheets but for graphite¹⁶, indicating that our

precursor material was in this form. For the graphene oxide sample, the peak on XRD appears at 6.3° , which leads to an interplanar distance of 14 \AA , almost five times the distance for graphene and graphite. That increase relates to the presence of oxygen groups between sheets¹⁶⁻¹⁸, corroborating FTIR and confirming the oxidation of graphene (or graphite) by the Hummers' Method.

Table 2 presents the XPS results from the Survey. A significant increase in oxygen atomic percent for the graphene oxide sample indicates the graphene's oxidation. As a result, the carbon content decreases. Nitrogen and sulfur are also present, which could be related to sample contamination by the atmosphere and solvent used to oxidize the graphene. Moreover, the C 1s fitting (Figure 4) confirms that the increase in oxygen atomic percent for the GO sample is related to the oxidation of graphene once the area contribution related to C-O covalent bonds increases significantly.

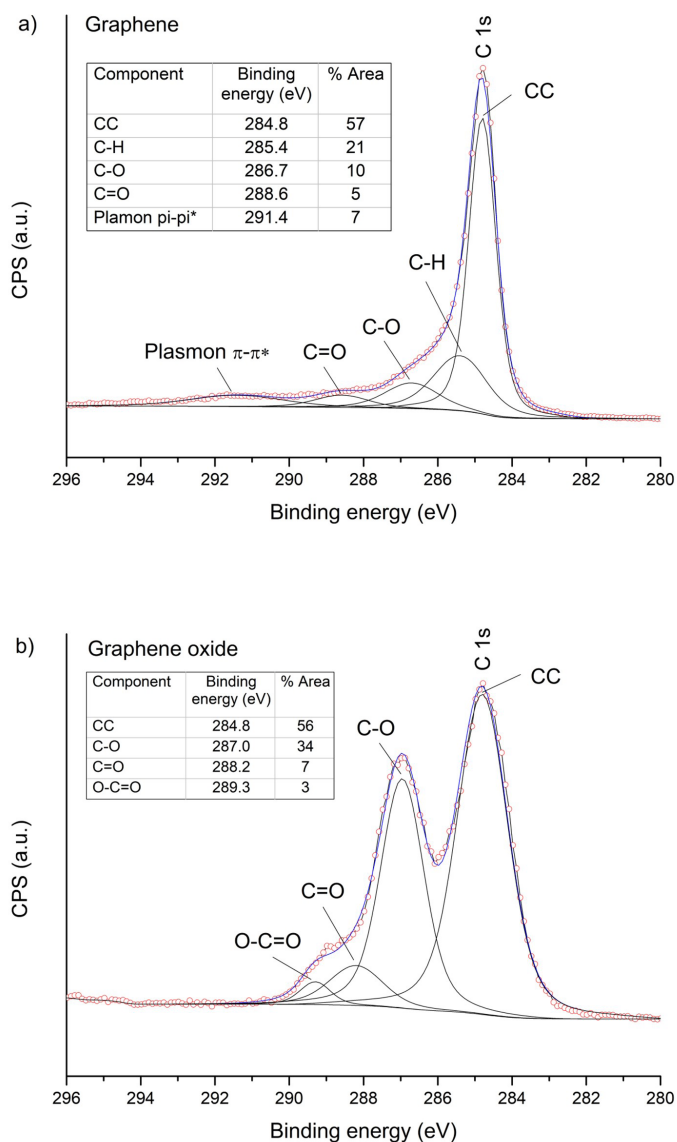


Figure 4. XPS C 1s fitting for a) graphene and b) graphene oxide samples, showing significant increase in C-O contribution after oxidation of graphene.

Table 2. XPS data for graphene and graphene oxide samples, obtained from Survey spectra.

	Atomic % (mean \pm standard deviation)			
	C 1s	O 1s	N 1s	S 2p
Graphene	94.3 \pm 0.4	3.6 \pm 0.1	2.1 \pm 0.3	-
Graphene oxide	65.3 \pm 0.1	31.0 \pm 0.5	1.4 \pm 0.4	2.2 \pm 0.1

3.2. Characterization of nanoparticle mixtures

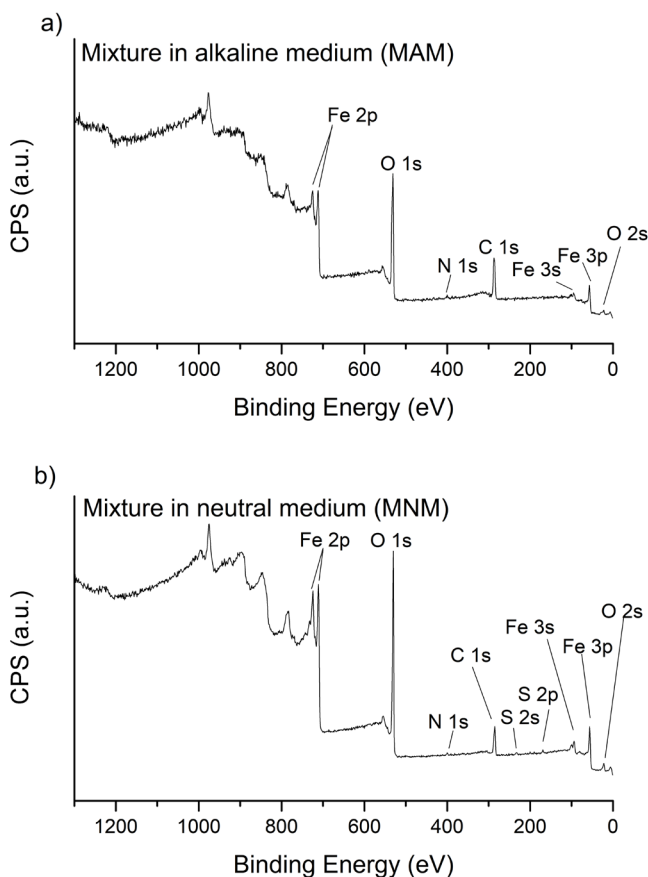
Figure 5 presents XPS survey spectra for both alkaline medium (MAM) and neutral medium (MNM) mixtures between the GO and the iron oxide (II). Iron, carbon, nitrogen, and oxygen are the elements identified in the chemical composition of both samples. The MNM sample also detected sulfur on the surface, probably from contamination throughout the graphene oxidation process. The atomic percentage of each element for both samples is shown in Table 3. Significant

differences were observed for the carbon and iron values: carbon quantity (in atomic %) was doubled in the MAM, as was the iron in the MNM sample. The decrease in iron quantities in the MAM process could be related to the hydrolysis and dissolution/redeposition reactions that may occur with iron oxide in an alkaline solution^{19,20}, indicating its solubilization, probably in the FeOH_2 form, more stable at alkaline pH and with a solubility of 0.72g/100mL²⁰. Although the MNM mixture presented higher quantities of Fe(II), it is also stable in aerated neutral media in the insoluble FeOOH form.

In Figure 6, TEM images evidence that a significant number of smaller-sized Fe(II) nanoparticles cover the reduced graphene oxide sheet for the MAM sample (Figures 6a and b). However, this is not observed in samples obtained using a neutral medium (Figures 6c and d), where iron oxide nanoparticles

Table 3. XPS data for mixture in alkaline medium and mixture in neutral medium of graphene oxide and iron oxide.

	Atomic % (mean \pm standard deviation)				
	C 1s	O 1s	N 1s	S 2p	Fe 2p
Mixture in alkaline medium	41.1 \pm 1.0	45.5 \pm 0.6	2.1 \pm 0.2	-	11.3 \pm 1.6
Mixture in neutral medium	25.5 \pm 2.2	51.6 \pm 2.3	1.3 \pm 0.2	1.2 \pm 0.5	20.4 \pm 4.1

**Figure 5.** XPS Survey spectra of a) MAM and b) MNM samples, related to mixtures between graphene oxide and Fe₂O₃ (II) nanoparticles.

are agglomerated in regions close to the graphene oxide but not on its surface. This result suggests that an alkaline medium is necessary to guarantee that the iron nanoparticles are on the surface of the oxide graphene, even when the precursors are nanoparticles. Our method differs from the one used by Barai et al.¹¹, who synthesized iron oxide using FeCl₂·xH₂O and FeCl₃ as precursors in the presence of graphene oxide. Furthermore, Figures 6c and d showed Fe(II) agglomerates, possibly due to the hygroscopic FeOOH. At the same time, in the MAM mixture (Figure 6a and b), Fe(II) solubilization caused a good dispersion of the remaining iron oxide on the graphene sheets.

3.3. Characterization of nanocomposites

Figure 7 shows the FEG-SEM images for the PP/HDPE blend and its nanocomposites. It is not possible to observe the nanoparticles in the images, so only the fracture surface and the dispersed phase will be analyzed. The blend presents a matrix-dispersed particle structure, i.e., continuous PP and dispersed HDPE particles (indicated by arrows). These images also show adhesion between the phases since pullout

voids cannot be observed. This behavior may be related to the polypropylene used in this work, a heterophasic ethylene-propylene copolymer. No significant differences in the blend morphology are observed with nanoparticles, as observed in our previous paper²¹. Most of the system has no significant differences in the HDPE phase size, which may indicate that the nanoparticles are preferentially located in the matrix phase (PP)²² or in the interface.

The DSC analysis is shown in Figure 8, and Table 4 summarizes characteristic temperatures and the degrees of crystallinity for each sample. The data in Table 5 show that the crystallization temperature did not suffer any change for both the HDPE and the PP phases. On the other hand, the melting temperature and the degree of crystallinity were lowered mainly for the dispersed phase of the HDPE. It is well known that PP and the HDPE could interfere with each other's crystallization²³⁻²⁷, so the presence of the nanoparticles in the blend interface could increase this interference since nucleation at the interface between the two components has been observed by different authors^{26,27}.

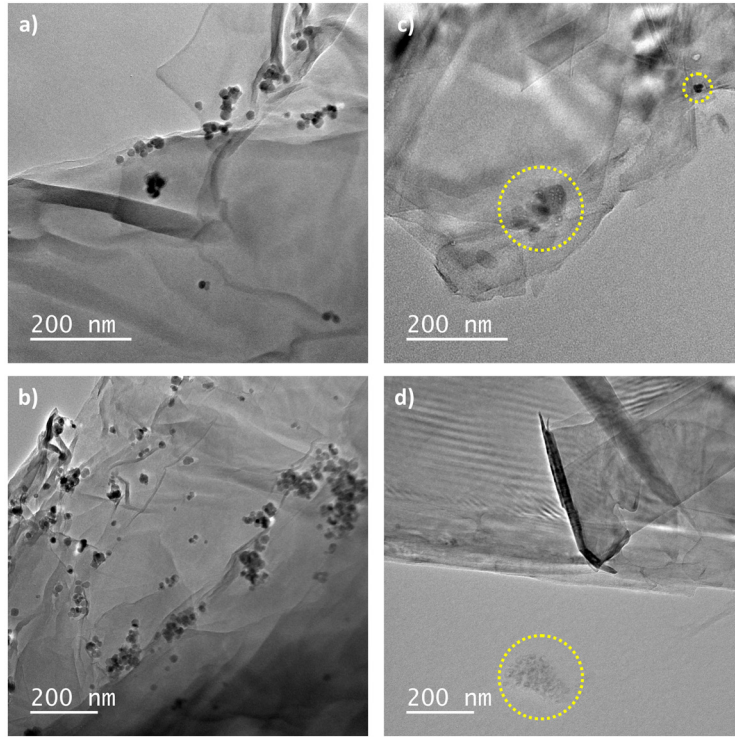


Figure 6. MET images for MAM (a and b) and MNM (c and d) samples, highlighting the Fe_3O_4 agglomerates for mixture conducted in neutral medium.

Table 4. Melting and crystallization temperatures, and degree of crystallinity for HDPE and PP phases in the PP/HDPE blend and nanocomposites.

System	T_c HDPE (°C)	T_c PP (°C)	T_m HDPE (°C)	T_m PP (°C)	X_c HDPE (%)	X_c PP (%)
PP/HDPE	119	162	149	182	48	27
NC_ Fe_3O_4	120	162	145	180	34	20
NC_GO	120	162	145	180	38	22
NC_MAM	119	161	146	182	37	26
NC_MNM	119	161	147	182	35	26

Table 5. Data summary of storage modulus and glass transition temperature for each sample. Values obtained through graphics from Figure 9.

Nanocomposite	E' (MPa) in -150 °C	E' (MPa) in -75 °C	E' (MPa) in 25 °C	T_g (°C) HDPE	T_g (°C) PP
PP/HDPE	3,006	1,738	75	-127	-7.3
NC_ Fe_3O_4	10,800	62,59	205	-144	-0.5
NC_GO	4,063	2,045	80	-132	-2.3
NC_MAM	687	423	40	-134	-4.8
NC_MNM	2,285	1,253	68	-137	-7.3

The DMA results can be seen in Figure 9, and the data are summarized in Table 5. The glass transition temperature values decrease for the discontinuous phase of the HDPE and increase for the continuous phase in all configurations of the nanocomposites. When the nanoparticles were preferentially located in the interface, it was expected that the T_g should be the same as those of the neat polymers if there is no interaction between the phases or move closer to each other when the nanoparticle act as a compatibilizer, improving the miscibility between the polymer phases. In this case, the T_g moved further from each other, meaning

nanoparticles somehow immobilized the PP chains while creating more free volume in which the HDPE chains could move. The sharpest modification is observed for the system with Fe_3O_4 (NC_ Fe_3O_4 sample). This shows more attractive surfaces between the Fe_3O_4 and PP phases. This behavior corroborates the storage modulus result. The highest E' value is observed in the Fe_3O_4 ternary system. This also may indicate that there are Fe_3O_4 nanoparticles in the PP phase.

In quaternary systems, a decrease in the storage modulus is observed, which is more significant in the system with the addition of the mixture conducted in an alkaline medium

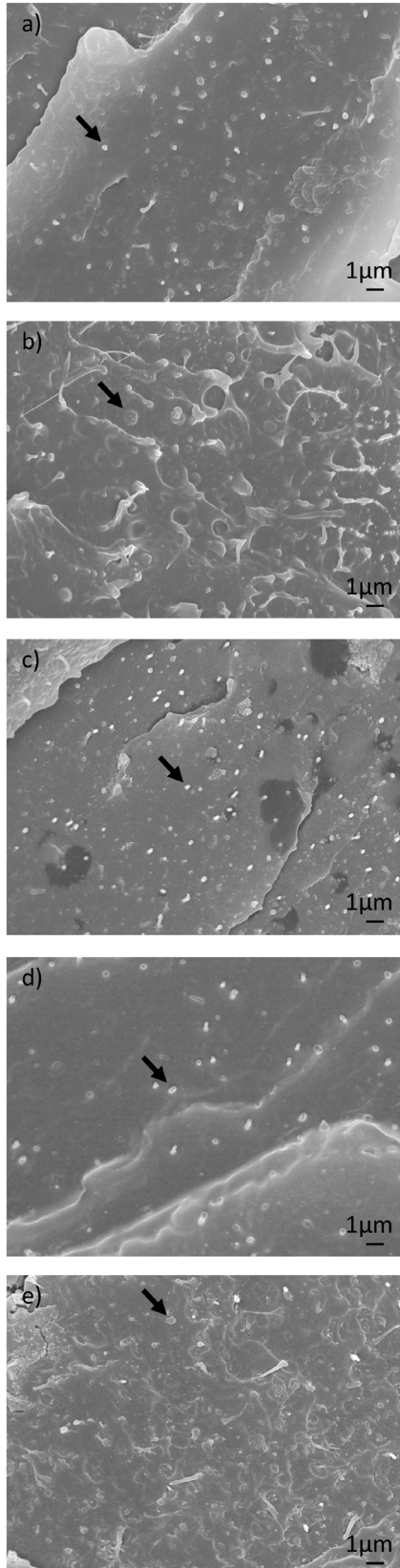


Figure 7. FEG-SEM images of a) PP/HDPE blend, and nanocomposites b) NC_Fe₃O₄; c) NC_GO; d) NC_MAM; and e) NC_MNM. Arrows pointed to HDPE dispersed phase.

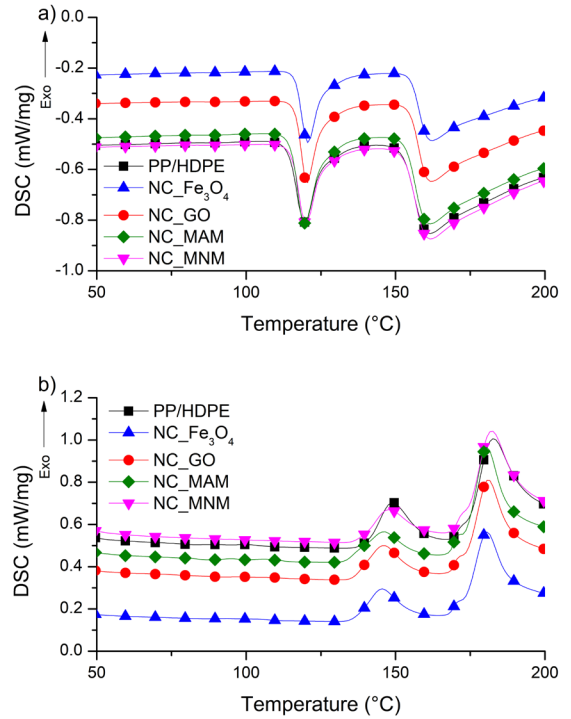


Figure 8. DSC curves of (a) heating and (b) cooling for the PP/HDPE blend and the nanocomposites.

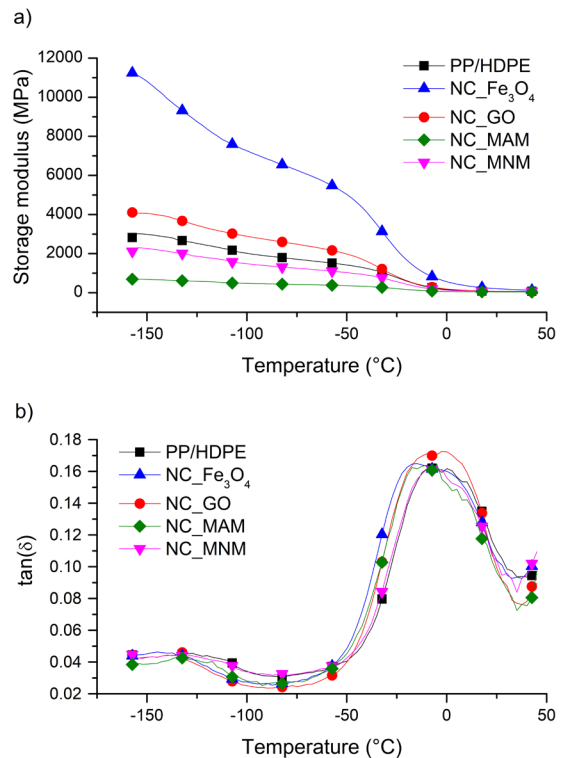


Figure 9. DMA results of the blend and nanocomposites: a) storage modulus (E') and b) $\tan\delta$ as a function of temperature.

(NC_MAM sample). The behavior of these systems can be linked to the amount of Fe₃O₄ in the mixture. According to the XPS results, the system with the highest amount of Fe₃O₄

nanoparticles (MNM sample) showed a minor reduction in the modulus. On the other hand, the NC_MAM sample, which has the highest amount of graphene oxide, showed the lowest E' value. Additionally, in the NC_MAM, the Fe_3O_4 nanoparticles were mainly on the oxide graphene surface, making it challenging to interact with the polymer. The results of the ternary systems show that Fe_3O_4 is more effective than graphene oxide in stress transfer and improves stiffness in PP/HDPE systems.

Figure 10 shows the variation of real permittivity (ϵ') with the frequency from the data obtained from the EIS analysis, and present the values obtained at 1 MHz, also known as the dielectric constant, for each sample.

Figure 10 show that higher dielectric constants were achieved after adding one nanoparticle: the dielectric constant almost doubled in the NC_ Fe_3O_4 (10.7) and tripled in the NC_GO sample (12.7). However, adding multiple nanoparticles does not positively affect the overall dielectric performance of the nanocomposite (NC_MAM, 6.8, and NC_MNM, 3.6, samples). This data was obtained in a frequency range characterized by the ionic polarization mechanism, which can be affected by carbon chains' stretching and elongation mechanism in polymeric blends³. Nanoparticles in the polymeric matrix add more polarization mechanisms than those already present in the carbon chains. So, it was expected that GO dispersion in the polymeric matrix had caused an increment in the capacity to store electrical energy by charge accumulation⁴. Similarly, iron oxide (II) adds more ionic polarization sites, improving charge accumulation through the material⁵. Comparing similar systems with the addition of graphene oxide²⁸ or iron oxide (II)²⁹ in PP blends a slight increase in the dielectric constant was observed: from 10 to 12.7 for NC_GO and from 5 to 10 for NC_ Fe_3O_4 samples. In both cases, the enhancement to dielectric constant values is explained by the polymeric matrix's high dispersion of the nanoparticles. This also promoted compatibilization and interfacial adhesion of different phases in the blend, observed by the microscopic analysis. This increment on interphase sites caused the insertion of new polarization mechanisms, which did not occur in the initial blend.

However, other effects should be considered when the quaternary composites are analyzed. Fe(II) in an aqueous solution may form metastable $FeOH^+$ and $Fe(OH)_2$ phases according to Ph and aerated conditions. In this work, for the preparation of nanocomposite mixtures, Fe(II) was submitted to neutral or alkaline Ph in the presence of oxygen, which led to the formation of different Fe(II) species. In fact, XPS results showed different atomic ratios of Fe/C for the MAM and MNM mixtures. And, of course, all these aspects influence the dielectric properties of the final nanocomposites.

Although the presence of nanoparticles promotes the formation of polarization mechanisms that contribute to the real part of permittivity, hydrophilic nanoparticles contribute to dielectric loss since they form mechanisms for the dissipation of electromagnetic energy. This effect was also observed in nanocomposites with PP and silica, where nanocomposites with hydrophilic silica presented more significant dielectric losses, leading to the understanding that the presence of water and the greater state of agglomeration of the particles restrict the movement of the dipoles³⁰. So, in the quaternary nanocomposites, both effects are present.

In some cases, the atomic ratio of different elements in the nanocomposites was used to help explain some properties, such as hydrophilicity³¹; therefore, the same logic will be applied here to elucidate the differences observed for the dielectric constants. In NC_MAM and NC_MNM cases, the dielectric constant did not increase because of the amount of hydrolyzed iron oxide dispersed through the graphene oxide sheet. As observed in the XPS analysis, the proportion between iron and carbon was significantly different for MAM and MNM mixtures. The MAM sample, with a higher proportion of carbon atoms and well-dispersed iron nanoparticles, presented a higher dielectric constant than the MNM sample. On the other hand, in the MNM sample, the higher content of hydrolyzed iron nanoparticles has reduced the GO dispersion in the polymer matrix, creating agglomerates that are not effective in improving electrical (or dielectric) properties.

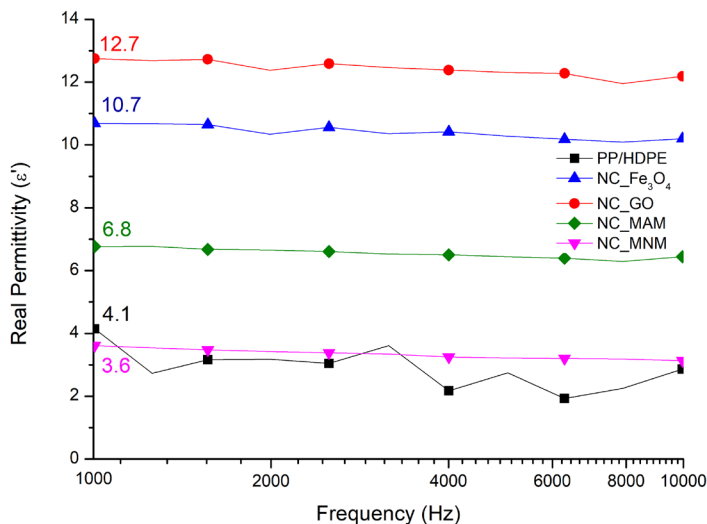


Figure 10. Dependence of real permittivity (ϵ') with the frequency calculated from EIS data, using Equation 2. Values inside the graph indicates ϵ' at 1 MHz.

4. Conclusions

The pH medium used to obtain mixtures of GO and Fe₃O₄ nanoparticles significantly impacts their chemical and morphological properties. The alkaline medium can promote hydrolysis and dissolution/redeposition reactions, decreasing the amount of iron nanoparticles in the final mixture. However, it is essential to use an alkaline medium to ensure the nanoparticle's dispersion and the iron nanoparticles remain on the surface of the GO.

In terms of nanocomposites, the addition of individual nanoparticles (ternary systems) yielded the best results. The Fe₃O₄ ternary system showed the highest storage modulus value, indicating that Fe₃O₄ is more effective than graphene oxide in stress transfer and improving stiffness in PP/HDPE systems. The dielectric constant almost doubled in the NC_Fe₃O₄ and tripled in the NC_GO sample. This increase in dielectric constant values may be related to the localization of nanoparticles in the polymeric matrix, which promotes compatibilization and interfacial adhesion of different phases in the blend. This, in turn, leads to the insertion of new polarization mechanisms that were not present in the initial blend.

In quaternary systems, the medium used also affects the nanocomposite properties. A decrease in the storage modulus was observed in both systems, but it was more significant when the mixture was added to an alkaline medium. This could be due to the iron nanoparticle quantities and their localization, which may delay stress transfer and improve stiffness in PP/HDPE systems. Nanoparticles in quaternary systems promote the formation of polarization mechanisms contributing to the real part of permittivity. Hydrophilic nanoparticles contribute to dielectric loss since they form mechanisms for the dissipation of electromagnetic energy. The presence of water and the greater state of agglomeration of the particles restrict the movement of the dipoles. The NC_MAM sample, with a higher proportion of carbon atoms and well-dispersed iron nanoparticles, showed a higher dielectric constant than the NC_MNM sample. On the other hand, in the NC_MNM sample, the higher content of hydrolyzed iron nanoparticles reduced the GO dispersion in the polymer matrix, creating agglomerates that are ineffective in improving electrical (or dielectric) properties.

5. Acknowledgments

This study was financed by FAPESC (PRONEM 2020TR716). The authors are thankful for the Multi-User Facility infrastructure of Santa Catarina State University's Technological Sciences Center. The authors would like to acknowledge the financial resources provided through CNPq, CAPES, and FAPESC.

6. References

- Arora P, Zhang ZJ. Battery separators. *Chem Rev.* 2004;104(10):4419-62. <http://dx.doi.org/10.1021/cr020738u>.
- Chung TCM. Functional polyolefins for energy applications. *Macromolecules.* 2013;46(17):6671-98. <http://dx.doi.org/10.1021/ma401244t>.
- Dabbak SZA, Illias HA, Ang BC, Latiff NAA, Makmud MZH. Electrical properties of polyethylene/polypropylene compounds for high-voltage insulation. *Energies.* 2018;11(6):1448. <http://dx.doi.org/10.3390/en11061448>.
- Deshmukh K, Ahamed MB, Pasha SKK, Deshmukh RR, Bhagat PR. Highly dispersible graphene oxide reinforced polypyrrole/polyvinyl alcohol blend nanocomposites with high dielectric constant and low dielectric loss. *RSC Adv.* 2015;5(76):61933-45. <http://dx.doi.org/10.1039/C5RA11242G>.
- Radoń A, Łukowiec D, Kremzer M, Miłkuła J, Włodarczyk P. Electrical conduction mechanism and dielectric properties of spherical shaped Fe₃O₄ nanoparticles synthesized by co-precipitation method. *Materials.* 2018;11(5):735. <http://dx.doi.org/10.3390/ma11050735>.
- Malles S, Jang W, Kim KH. Facile synthesis of cube-like Fe₃O₄-graphene oxide nanocomposites with excellent microwave absorption performance. *Phys Lett A.* 2021;389:127069. <http://dx.doi.org/10.1016/j.physleta.2020.127069>.
- Arshad A, Iqbal J, Mansoor Q. Graphene/Fe₃O₄ nanocomposite: solar light driven Fenton like reaction for decontamination of water and inhibition of bacterial growth. *Appl Surf Sci.* 2019;474:57-65. <http://dx.doi.org/10.1016/j.apsusc.2018.05.046>.
- Hatel R, Goumri M, Ratier B, Baitoul M. Graphene derivatives/Fe₃O₄/polymer nanocomposite films: optical and electrical properties. *Mater Chem Phys.* 2017;193:156-63. <http://dx.doi.org/10.1016/j.matchemphys.2017.02.013>.
- Sharmila TKB, Antony JV, Jayakrishnan MP, Beegum PMS, Thachil ET. Mechanical, thermal and dielectric properties of hybrid composites of epoxy and reduced graphene oxide/iron oxide. *Mater Des.* 2016;90:66-75. <http://dx.doi.org/10.1016/j.matdes.2015.10.055>.
- Jayakumar OD, Abdelhamid EH, Kotari V, Mandal BP, Rao R, Jagannath J, et al. Fabrication of flexible and self-standing inorganic-organic three phase magneto-dielectric PVDF based multiferroic nanocomposite films through a small loading of graphene oxide (GO) and Fe₃O₄ nanoparticles. *Dalton Trans.* 2015;44(36):15872-81. <http://dx.doi.org/10.1039/C5DT01509J>.
- Barai DP, Bhanvase BA, Saharan VK. Reduced graphene oxide-Fe₃O₄ nanocomposite based nanofluids: study on ultrasonic assisted synthesis, thermal conductivity, rheology, and convective heat transfer. *Ind Eng Chem Res.* 2019;58(19):8349-69. <http://dx.doi.org/10.1021/acs.iecr.8b05733>.
- Marcano DC, Kosynkin DV, Berlin JM, Sinitskii A, Sun Z, Slesarev A, et al. Improved synthesis of graphene oxide. *ACS Nano.* 2010;4(8):4806-14. <http://dx.doi.org/10.1021/nn1006368>.
- Jose S, Aprem AS, Francis B, Chandy MC, Werner P, Alstaedt V, et al. Phase morphology, crystallisation behaviour and mechanical properties of isotactic polypropylene/high density polyethylene blends. *Eur Polym J.* 2004;40(9):2105-15. <http://dx.doi.org/10.1016/j.eurpolymj.2004.02.026>.
- Zankana MM, Al-dalawy SM, Barzinjy AA. Synthesis and characterization of bio-nanocomposites: functionalization of graphene oxide with a biocompatible amino acid. *Hybrid Adv.* 2023;3:100070. <http://dx.doi.org/10.1016/j.hybadv.2023.100070>.
- Alkhouzaam A, Qiblawey H, Khraisheh M, Atieh M, Al-Ghouti M. Synthesis of graphene oxides particle of high oxidation degree using a modified Hummers method. *Ceram Int.* 2020;46(15):23997-4007. <http://dx.doi.org/10.1016/j.ceramint.2020.06.177>.
- Sibirian R, Sihotang H, Raja SL, Supeno M, Simanjuntak C. New route to synthesize of graphene nano sheets. *Orient J Chem.* 2018;34(1):182-7. <http://dx.doi.org/10.13005/ojc/340120>.
- Johra FT, Lee JW, Jung WG. Facile and safe graphene preparation on solution based platform. *J Ind Eng Chem.* 2014;20(5):2883-7. <http://dx.doi.org/10.1016/j.jiec.2013.11.022>.
- Krishnamoorthy K, Veerapandian M, Yun K, Kim SJ. The chemical and structural analysis of graphene oxide with different degrees of oxidation. *Carbon.* 2013;53:38-49. <http://dx.doi.org/10.1016/j.carbon.2012.10.013>.

19. Lopes DV, Quina MJ, Frade JR, Kovalevsky AV. Prospects and challenges of the electrochemical reduction of iron oxides in alkaline media for steel production. *Front Mater.* 2022;9:1010156. <http://dx.doi.org/10.3389/fmats.2022.1010156>.
20. Duarte HA. Ferro: um elemento químico estratégico que permeia história, economia e sociedade. *Quim Nova.* 2019;42(10):1146-53. <http://dx.doi.org/10.21577/0100-4042.20170443>.
21. Carvalho D, Becker D, Dalmolin C. Effect of carbon nanotube location and dispersed phase on the dielectric properties of polypropylene/high-density polyethylene/carbon nanotube nanodielectrics. *J Appl Polym Sci.* 2022;139(29):e52656. <http://dx.doi.org/10.1002/app.52656>.
22. Zou H, Wang K, Zhang Q, Fu Q. A change of phase morphology in poly(p-phenylene sulfide)/polyamide 66 blends induced by adding multi-walled carbon nanotubes. *Polymer.* 2006;47(22):7821-6. <http://dx.doi.org/10.1016/j.polymer.2006.09.008>.
23. Mastalygina EE, Popov AA, Kolesnikova NN, Karpova S. Morphology, thermal behaviour and dynamic properties of the blends based on isotactic polypropylene and low-density polyethylene. *Int J Plast Technol.* 2015;19(1):68-83. <http://dx.doi.org/10.1007/s12588-015-9112-5>.
24. Villers D, Dosiere M, Paternostre L. New dynamical effects in spherulitic growth. *Polymer.* 1994;35(8):1586-92. [http://dx.doi.org/10.1016/0032-3861\(94\)90831-1](http://dx.doi.org/10.1016/0032-3861(94)90831-1).
25. Dong L, Olley RH, Bassett DC. On morphology and the competition between crystallization and phase separation in polypropylene–polyethylene blends. *J Mater Sci.* 1998;33(16):4043-8. <http://dx.doi.org/10.1023/A:1004474902723>.
26. Góra M, Coba-Daza S, Carmeli E, Tranchida D, Albrecht A, Müller AJ, et al. Surface-enhanced nucleation in immiscible polypropylene and polyethylene blends: the effect of polyethylene chain regularity. *Polymer.* 2023;282:126180. <http://dx.doi.org/10.1016/j.polymer.2023.126180>.
27. Huang DE, Kotula AP, Snyder CR, Migler KB. Crystallization kinetics in an immiscible polyolefin Blend. *Macromolecules.* 2022;55(24):10921-32. <http://dx.doi.org/10.1021/acs.macromol.2c01691>.
28. Wang D, Zhang X, Zha JW, Zhao J, Dang ZM, Hu G-H. Dielectric properties of reduced graphene oxide/polypropylene composites with ultralow percolation threshold. *Polymer.* 2013;54(7):1916-22. <http://dx.doi.org/10.1016/j.polymer.2013.02.012>.
29. Ahangaran F, Hassanzadeh A, Nouri S, Neisiany RE. Investigation of thermal and dielectric properties of Fe₃O₄/high-density polyethylene nanocomposites. *J Compos Mater.* 2017;51(28):3923-9. <http://dx.doi.org/10.1177/0021998317695419>.
30. Hui L, Schadler SL, Nelson JK. The influence of moisture on the electrical properties of crosslinked polyethylene/silica nanocomposites. *IEEE Trans Dielectr Electr Insul.* 2013;20(2):641-53.
31. Al-Gaashani R, Najjar A, Zakaria Y, Mansour S, Atieh MA. XPS and structural studies of high quality graphene oxide and reduced graphene oxide prepared by different chemical oxidation methods. *Ceram Int.* 2019;45(11):14439-48. <http://dx.doi.org/10.1016/j.ceramint.2019.04.165>.